Synthesis, microstructure evolution, and mechanical properties of $(Cr_{1-x}V_x)_2AlC$ ceramics by in situ hot-pressing method

Jianfeng Zhu, Hao Jiang,[a] Fen Wang, and Qi Ma
Key Laboratory of Auxiliary Chemistry & Technology for Chemical Industry, Ministry of Education, Shaanxi University of Science and Technology, Xi'an 710021, China

(Received 15 November 2013; accepted 8 April 2014)

Nearly dense and almost single-phase bulk $(Cr_{1-x}V_x)_2AlC$ (x = 0, 0.25, 0.5, 0.75, and 1.0) ceramics were successfully fabricated by in situ hot-pressing method using Cr, V, Al, and C powders as raw materials. A possible synthesis mechanism was proposed to explain the formation of $(Cr_{1-x}V_x)_2AlC$ solid solutions. The lattice parameters, microstructure, and mechanical properties of the $(Cr_{1-x}V_x)_2AlC$ ceramics were investigated in detail. The results indicated that the lattice parameters increased with the substitution of Cr by V and the aspect ratio of the grain changed from 1.4 to 3.2. The dependence of the mechanical properties on the V content was a single-peak type. The $(Cr_{0.5}V_{0.5})_2AlC$ ceramic possessed the optimal mechanical performance and its Vickers hardness, flexural strength, and fracture toughness reached the maximum values of 5.18 GPa, 402 MPa, 5.91 MPa $m^{1/2}$, respectively, due to the solid solution effect. The energy-consuming mechanisms of the material were also discussed.

I. INTRODUCTION

The $M_{n+1}AX_n$ compounds, where M is an early transition metal, A is an element of IIIA or IVA, X is either C or N, and n = 1–6, are a class of hexagonal-structure ternary carbides and nitrides which have attracted extensive attention owing to the combination of the excellent properties of both metals and ceramics.[1–3] Like metals, they have high thermal and electrical conductivity,[4] excellent thermal shock resistance and good machinability; like ceramics, they possess high strength,[5] high melting point, excellent high-temperature oxidation resistance,[6,7] and good thermal stability.[8,9]

Moreover, the solid solution based on the MAX phases can be formed by the substitution of elements on M, A, or X site. Such as $(Cr_{1-x}V_x)_2AlC$,[10] $(Ti_{1-x}Nb_x)_2AlC$,[11] $(Ti_{1-x}V_x)_2AlC$[12] and $Ti_2Al(C_{0.5}N_{0.5})$[13] in the so-called 211 phase, and $Ti_3Si_xAl_{1-x}C_2$,[14] $Ti_3Al_xSn_{1-x}C_2$,[15] $Ti_3Ge_xSi_{1-x}C_2$[16] and $Ti_3Al(C_{0.5}N_{0.5})_2$[17] in 312 phase. Solid solution treatment is considered as an effective way to optimize the properties of $M_{n+1}AX_n$ compounds. For example, Wang and Zhou[18] investigated the elastic stiffness and electronic band structure of $M_xM'_{2-x}AlC$ (M and M′ = Ti, V, Cr) phases by the ab initio pseudopotential total energy method. They found that the second-order elastic constant c_{44}, a hardness predictor, reached a maximum value as the valence electron concentration (VEC) was in the range 8.4–8.6. So it was predicted that the mechanical properties of $M_xM'_{2-x}AlC$ would be improved by forming solid solutions. As a member of $M_xM'_{2-x}AlC$, $(Cr_{1-x}V_x)_2AlC$ is of great interest to us. For this system, both experimental and theoretical studies had been conducted in the past. Schuster et al.[2] first synthesized $(Cr_{0.75},V_{0.25})_2AlC$, $(Cr_{0.5},V_{0.5})_2AlC$, and $(Cr_{0.25},V_{0.75})_2AlC$ solid solutions by annealing a series of Cr_2AlC and V_2AlC powder mixtures in appropriate proportions at 1000 °C for 170 h. Their results showed that Cr_2AlC and V_2AlC could form a complete series of mutual solid solutions. Sun et al.[19] explored the solubility of $M_xM'_{2-x}AlC$ (M and M′ = Ti, V, Cr) by first principle calculation method. Therein, the solubility of the $(Cr_{1-x}V_x)_2AlC$ system was also proved theoretically, which explained the results in Schuster's work. And then, Tian et al.[10] synthesized several $(Cr_{1-x}V_x)_2AlC$ (x = 0, 0.1, 0.25, and 0.5) by the pulse discharge sintering (PDS) technique using Cr, V, Al, and C powders and reported the hardness and thermal conductivity of the products. Subsequently, Yeh and Yang[20] successfully fabricated $(Cr,V)_2AlC$ with Al_2O_3 addition based on chromium (III) oxide (Cr_2O_3)–vanadium pentoxide (V_2O_5)–aluminum(Al)–aluminum carbide (Al_4C_3) system by self-propagating high-temperature synthesis (SHS) method involving aluminothermic reduction. However, there is less systematic investigation of the microstructure, solid solution effect, and mechanical properties of bulk $(Cr_{1-x}V_x)_2AlC$ continuous solid solutions.

Generally, sintering method is the dominant process for the tailoring of the microstructures and properties of the $(Cr_{1-x}V_x)_2AlC$ solid solutions. As a promising alternative method, the in situ hot-pressing sintering has many characteristics such as in situ solid solution

[a]Address all correspondence to this author.
e-mail: haojiangcd@163.com
DOI: 10.1557/jmr.2014.91

 © Materials Research Society 2014

https://doi.org/10.1557/jmr.2014.91 Published online by Cambridge University Press

reaction at relatively low temperatures to achieve considerably high-density and high-purity ceramics within short sintering time, thus manifesting distinct advantages as compared with the traditional methods.

Therefore, the purpose of this work is 2-fold; First, to fabricate dense and high purity $(Cr_{1-x}V_x)_2AlC$ (x = 0, 0.25, 0.5, 0.75, and 1.0) ceramics using an in situ hot-pressing process and study the synthesis mechanism. Second, to investigate the lattice parameters, microstructure, mechanical properties, and solid solution effect of bulk $(Cr_{1-x}V_x)_2AlC$ ceramics.

II. EXPERIMENTAL PROCEDURES

Powders (all from Xing Rong Yuan Technology Co., Ltd., Beijing, China) of Cr (99.9% in purity, 200 mesh), V (99.9% in purity, 200 mesh), Al (99.5% in purity, 200 mesh) and carbon black (99.5% in purity, 200 mesh) were used as starting materials. For the preparation of $(Cr_{1-x}V_x)_2AlC$ solid solutions, the powder mixtures containing Cr, V, Al, and C were formulated with stoichiometry. Extra 10 wt% Al was used to compensate for the loss of Al during the sintering process. And the detailed component description of the samples is listed in Table I.

The powder mixture was ball milled in alcohol for 1 h and then dried at less than 50 °C for several hours. Then the dried powders were compacted uniaxially at 10 MPa in a graphite mold with a protective layer of boron nitride (BN). The compacted samples were hot pressed in vacuum (less than 6.0×10^{-2} Pa) at a rate of 5 °C/min to 1400 °C, and held for 2 h under a pressure of 16 MPa. Finally, the samples were cooled down to room temperature in the furnace. Before examination, the surface of the samples was ground to remove graphite contamination layers. To expose the grains, the surface of the samples was polished and etched using a mixture of hydrofluouric acid, nitric acid, and water ($HF:HNO_3:H_2O$) solution with a 1:1:1 volumetric ratio. The phase formation of the sintered bulks was identified by x-ray diffraction (XRD) with Cu K_α radiation (D/max-2200PCX) at a scanning speed of 0.02°/step. The microstructure of the samples was investigated by scanning electron microscope (SEM, HITACH, FE-S4800, Japan) and energy dispersive spectroscopy (EDS).

The measurements of all the mechanical properties were performed at room temperature by averaging six individual measurements. The density of $(Cr_{1-x}V_x)_2AlC$ samples was measured by the Archimedes method. Vickers hardness measurements were conducted on the HXD-1000 tester (Shanghai second optical Ltd., China) with a diamond indenter under a 1000 N load for 15 s. The three-point flexural strength test was conducted using 3 mm × 4 mm × 36 mm specimens by the PT-1036PC material tester (Perfect Instrument Co. Ltd., Taiwan, China), with a span of 20 mm and at a cross-head speed of 0.5 mm/min. The fracture toughness test was carried out by the single edge notched beam (SENB) method using 2 mm × 4 mm × 36 mm specimens with a notch depth of $0.4h$ (h is the height of specimen), at a cross-head speed of 0.05 mm/min, with a loading span of 20 mm. The flexural strength and fracture toughness of the specimens were calculated by the following Eqs. (1) and (2), respectively:

$$\sigma = 3PL/2bh^2 \quad , \tag{1}$$

where P is the breaking load of the specimen, and L, b, and h denote the length, width, and height, respectively.

$$K_{IC} = Y \times 3PLa^{1/2} \Big/ \left(2bh^2\right) \quad , \tag{2}$$

where Y is a geometrical factor, and a is the notch length.

TABLE I. The compositions of the $(Cr_{1-x}V_x)_2AlC$ (x = 0, 0.25, 0.5, 0.75, 1.0) mutual solid solutions (mole ratio).

Sample	Cr	V	Al	C
Cr_2AlC	2	0	1.1	1
$(Cr_{0.75}V_{0.25})_2AlC$	1.5	0.5	1.1	1
$(Cr_{0.5}V_{0.5})_2AlC$	1	1	1.1	1
$(Cr_{0.25}V_{0.75})_2AlC$	0.5	1.5	1.1	1
V_2AlC	0	2	1.1	1

III. RESULTS AND DISCUSSION

Figure 1 shows the XRD patterns of hot-pressed sample of $(Cr_{0.5}V_{0.5})_2AlC$ solid solution sintered at different temperatures ranging from 500 °C to 1400 °C for 2 h. As shown in Fig. 1(a), only Cr, V, and Al phases were detected in the samples sintered at 500 °C. No diffraction peaks of C were observed because amorphous carbon black was used in this work. As the sintering temperature increased to 700 °C, which was higher than the melting point of aluminum ~660 °C [Fig. 1(b)], the diffraction peaks of Al disappeared completely and those of Cr and V became weaker. Al_8Cr_5 and Al_3V phases were detected noticeably, suggesting the reactions of Al with Cr and V to form Cr–Al and V–Al intermetallics, respectively according to Eqs. (3) and (4). Besides, a small amount of Cr_2Al was also detected, indicating the reaction of Al_8Cr_5 with Cr according to Eq. (5).

As shown in Fig. 1(c), all the diffraction peaks of Cr, V, Al_8Cr_5, and Al_3V disappeared at 900 °C, while Al_8V_5 became the main phase and the diffraction peak intensity of the Cr_2Al phase increased noticeably. It was indicated that the Cr, V, Al_8Cr_5, and Al_3V were exhausted completely to form the intermetallic equilibrium phases, Cr_2Al and Al_8V_5, according to Eqs. (5) and (6), respectively. As the temperature reached 1100 °C [Fig. 1(d)], V_2AlC and Cr_2AlC appeared while the content of the Al_8V_5 and Cr_2Al

https://doi.org/10.1557/jmr.2014.91 Published online by Cambridge University Press

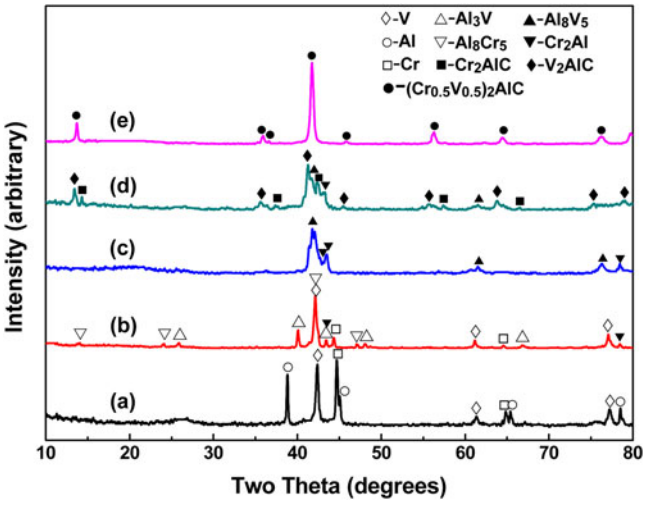


FIG. 1. XRD patterns of hot-pressed $(Cr_{0.5}V_{0.5})_2AlC$ solid solution at different temperatures: (a) 500 °C; (b) 700 °C; (c) 900 °C; (d) 1100 °C; (e) 1400 °C.

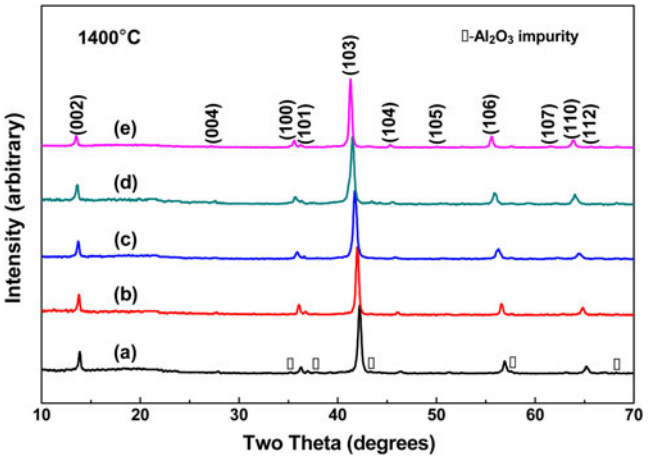


FIG. 2. XRD patterns for (a) Cr_2AlC; (b) $(Cr_{0.75}V_{0.25})_2AlC$; (c) $(Cr_{0.5}V_{0.5})_2AlC$; (d) $(Cr_{0.25}V_{0.75})_2AlC$; (e) V_2AlC.

decreased, implying that the two MAX phases were formed by the reaction among C, Al_8V_5, and Cr_2Al according to Eqs. (7) and (8). When the temperature further increased to 1400 °C [Fig. 1(e)], single-phase $(Cr_{0.5}V_{0.5})_2AlC$ solid solution was formed by the reaction between Cr_2AlC and V_2AlC according to Eq. (9). The reaction Eqs. (3)–(9) are summarized as follows:

$$8Al + 5Cr \rightarrow Al_8Cr_5 \quad , \tag{3}$$

$$3Al + V \rightarrow Al_3V \quad , \tag{4}$$

$$11Cr + Al_8Cr_5 \rightarrow 8Cr_2Al \quad , \tag{5}$$

$$7V + 8Al_3V \rightarrow 3Al_8V_5 \quad , \tag{6}$$

$$Cr_2Al + C \rightarrow Cr_2AlC \quad , \tag{7}$$

$$2Al_8V_5 + 5C \rightarrow 5V_2AlC + 11Al \quad , \tag{8}$$

$$Cr_2AlC + V_2AlC \rightarrow 2(Cr_{0.5}V_{0.5})_2AlC \quad . \tag{9}$$

The XRD patterns of the $(Cr_{1-x}V_x)_2AlC$ solid solutions with the V content increased from 0 to 100 at.% sintered at 1400 °C for 2 h are shown in Fig. 2. The samples were only composed of $(Cr_{1-x}V_x)_2AlC$ and trace amount of aluminum oxide (Al_2O_3). The diffraction peaks of the main phases were very sharp, suggesting a high crystallinity of the grains obtained. And the Al_2O_3 impurity was commonly observed in synthetic Al-containing MAX phases and their solid solutions.[11,13,15,21] As shown in the figure, all the detected diffraction peaks of the solid solutions were marked on the basis of the crystal structure of Cr_2AlC [Joint Committee on Power Diffraction Standards (JCPDS) card No. 29-0017]. It could also be found that the diffraction peaks shifted to left gradually with the increase of V content. For instance, the diffraction angle of (103) crystal face changed gradually from 42.22° for Cr_2AlC to 41.30° for V_2AlC with the substitution of Cr. It was attributed to the increment of lattice parameters as replacing Cr by V on the M site of $(Cr_{1-x}V_x)_2AlC$.

For accurately describing the changes in the lattice parameters of the solid solutions, Rietveld cell refinement of the diffraction patterns was conducted by MID jade5 software using Cr_2AlC as the structural model. The final reliability factors (R_p and R_{wp}) are less than 10% in all the composition range, suggesting the sufficient accuracy of the refinement. As shown in Fig. 3(a), when the V content on the M site increased from 0 to 100 at.%, the lattice constant a changed linearly from 2.8572 Å to 2.9133 Å, and c increased significantly from 12.8188 Å to 13.1394 Å. The reason for the increment of lattice parameters was the larger radius size of the V atom (r_{Cr} = 166 pm, r_V = 171 pm).[22] The more significant increment in constant c was due to the weaker electronic bonding in the c direction. For comparison, the calculated parameters and c/a ratios of $(Cr_{1-x}V_x)_2AlC$ solid solutions with different V content in Ref. 19 are plotted in Fig. 3(b). The change trend of lattice parameters in the present work was similar to that in the literature. However, the two dependences of c/a ratios on V content were different. In our work, with the substitution of Cr by V, the c/a ratio increased progressively without any peak from 4.4865 to 4.5101, which was attributed to the higher changing rate of c. For a detailed and visual display, all the data are also listed in Table II.

Figure 4 presents a typical SEM micrograph together with EDS spectra of the polished and etched surface of $(Cr_{0.5}V_{0.5})_2AlC$ prepared at 1400 °C for 2 h. As shown in Fig. 4(a), the average size (the average of two times length and one time width) of gray grains was about 18.7 μm. As shown in Fig. 4(b), the atomic ratio of Cr:V:Al of the grain

https://doi.org/10.1557/jmr.2014.91 Published online by Cambridge University Press

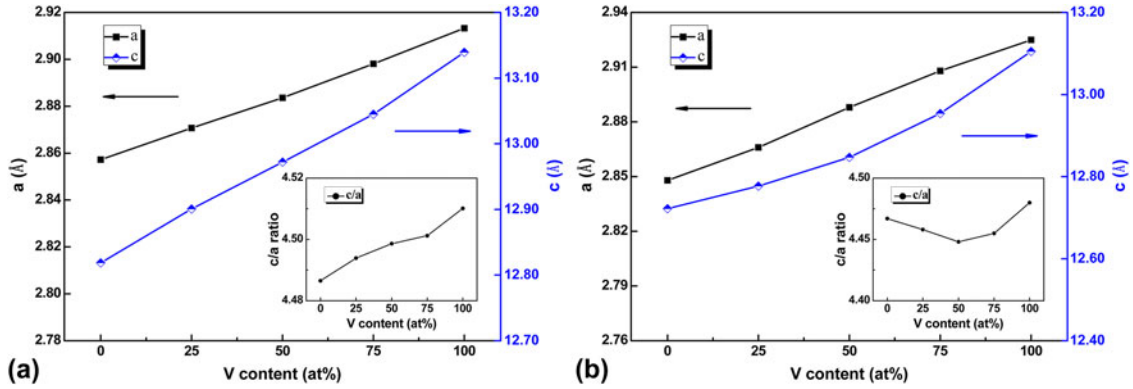


FIG. 3. Calculated lattice parameters and *c*/*a* ratios for $(Cr_{1-x}V_x)_2AlC$ solid solutions with different V content on the M site from (a) the present work and (b) Ref. 19.

TABLE II. Summary of the measured properties of the $(Cr_{1-x}V_x)_2AlC$ solid solutions (*a* and *c*, lattice parameters; R_p and R_{wp}, reliability factors; d_m, measured density; d_c, calculated density; d_r, relative density).

	Present work								Reference 19			Reference 10	
Item	*a* (Å)	*c* (Å)	*c*/*a*	R_p (%)	R_{wp} (%)	d_m (g/cm^3)	d_c (g/cm^3)	d_r (%)	*a* (Å)	*c* (Å)	*c*/*a*	d_m (g/cm^3)	d_r (%)
Cr_2AlC	2.8572	12.8188	4.4865	7.57	9.48	4.967 ± 0.005	5.231	95.0	2.848	12.722	4.467	5.14	98.3
$(Cr_{0.75}V_{0.25})_2AlC$	2.8707	12.9006	4.4939	7.23	9.81	4.904 ± 0.007	5.138	95.4	2.866	12.777	4.458	5.03	98.1
$(Cr_{0.5}V_{0.5})_2AlC$	2.8836	12.9722	4.4986	7.73	9.61	4.876 ± 0.006	5.046	96.6	2.888	12.847	4.448	4.95	98.2
$(Cr_{0.25}V_{0.75})_2AlC$	2.8981	13.0449	4.5012	7.34	9.89	4.815 ± 0.008	4.980	96.7	2.908	12.954	4.455	...	...
V_2AlC	2.9133	13.1394	4.5101	6.95	9.36	4.768 ± 0.006	4.874	97.8	2.925	13.105	4.480	...	...

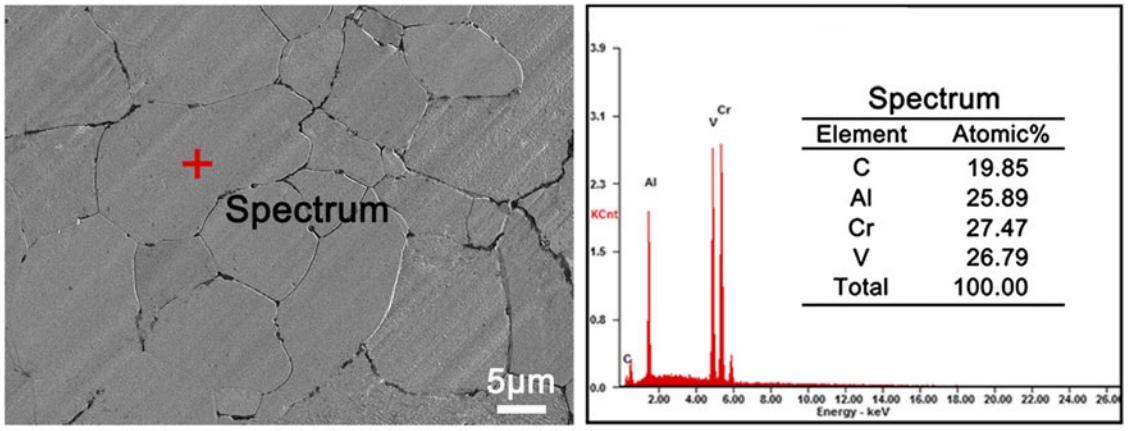


FIG. 4. (a) SEM micrograph of $(Cr_{0.5}V_{0.5})_2AlC$ polished and etched surface; (b) EDS spectra.

[marked as spectrum in Fig. 4(a)] was 27.47:26.79:25.89, which was quite close to the theoretical value of 1:1:1. The content of C in the result was slightly lower than the theoretical value, because the mass of C atom was too light to be detected accurately by the EDS analysis. Although it was difficult to quantify the composition in the products accurately, combined with the XRD result in Figs. 1 and 2, it was confirmed that the plate-like grains were $(Cr_{0.5}V_{0.5})_2AlC$ phase.

Figure 5(a) presents the SEM micrograph of a typical fracture surface of the $(Cr_{0.5}V_{0.5})_2AlC$ sample. As shown in the figures, cleavage planes with the typical laminated structure were displayed. And transgranular and intergranular cracks were clearly observed, indicating the occurrence of both fracture modes in the $(Cr_{1-x}V_x)_2AlC$ solid solutions. Figure 5(b) demonstrates the high magnification image of the rectangular region in Fig. 5(a). Like other $M_{n+1}AX_n$ phase materials,[23–25] Kink bands, step-like

https://doi.org/10.1557/jmr.2014.91 Published online by Cambridge University Press

delamination and lamellar tearing were observed in the sample. The multiple microscopic deformation and damage modes were favorable for absorption of more energy during the fracture process. As a result, the energy-consuming mechanisms in the $(Cr_{1-x}V_x)_2AlC$ solid solutions would lead to high toughness and ductility.

Figure 6 demonstrates the SEM micrographs of the polished and etched surfaces of the $(Cr_{1-x}V_x)_2AlC$ ceramics sintered at 1400 °C for 2 h. The average grain size of these solid solutions was about 17.9–19.5 μm (see Table III). No obvious large pores were found on the surfaces, which would contribute to excellent mechanical properties. More remarkably, as a result of the increasing aspect ratio (Table III), the shape of $(Cr_{1-x}V_x)_2AlC$ grains changed from equiaxial (for Cr_2AlC, as shown in Fig. 6(a)) to elongated morphology (for V_2AlC, as shown in Fig. 6(e)) with substitution of Cr by V. In the light of the previous literature, the crystal habits of Cr_2AlC and V_2AlC were different, i.e., Cr_2AlC generally crystallized to be hexagonal grains,[4,8] while V_2AlC crystallized to be long-columnar ones.[26] So it was indicated that the V content had an obvious effect on the crystal habit of $(Cr_{1-x}V_x)_2AlC$ solid solutions.

The density and Vickers hardness of $(Cr_{1-x}V_x)_2AlC$ ceramics with different V content are shown in Fig. 7. Apparently, the density decreased from 4.967 to 4.768 g/cm^3 as the V content increased from 0 to 100 at. %, which was ascribed to the incorporation of relatively light V into Cr_2AlC and the expansion of crystal structure of the solid solutions. As illustrated in Table II, The relative density of all products was 95.0–97.8% of the calculated one with XRD patterns. But compared with the results of several bulk $(Cr_{1-x}V_x)_2AlC$ in Ref. 10, the values in the present work were slightly smaller. This was correlated with the lower applied pressure in our synthetic process (50 and 30 MPa in Ref. 10). Also as depicted in Fig. 7, the change of Vickers hardness with the V content was shown as a single-peak curve, and it

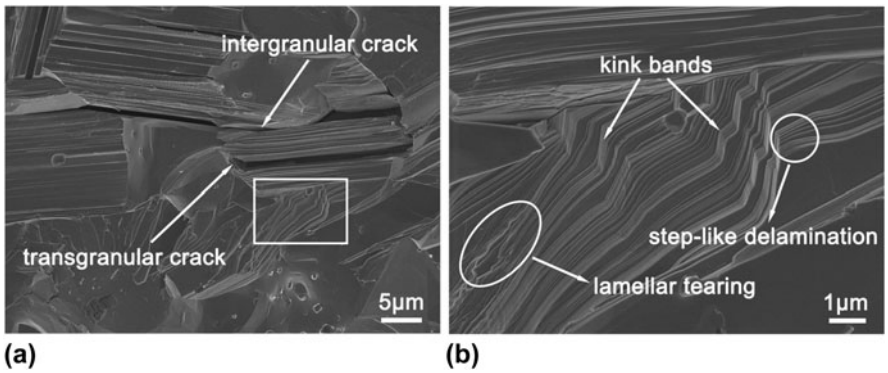


FIG. 5. (a) SEM micrograph of a typical fracture surface of $(Cr_{0.5}V_{0.5})_2AlC$ sample; (b) the enlarged image of the rectangular region from (a).

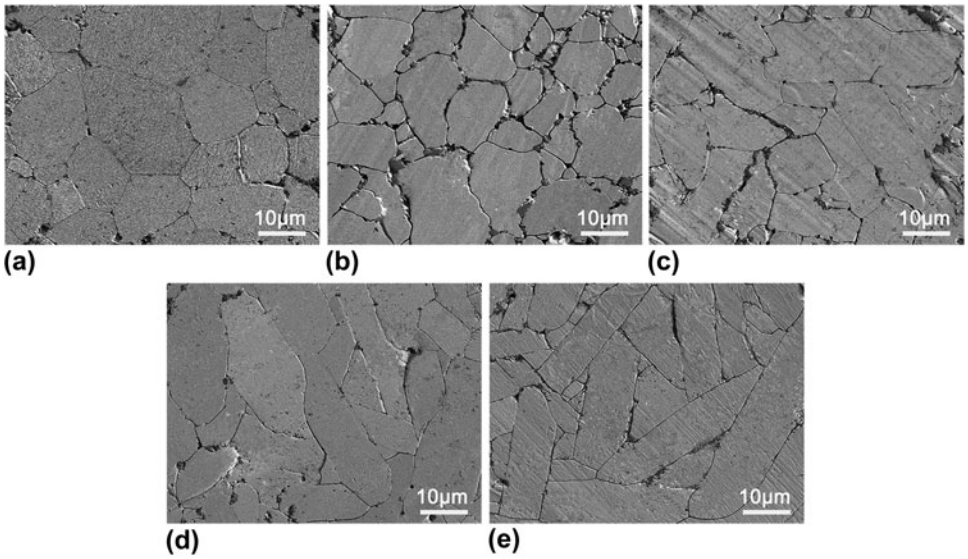


FIG. 6. SEM micrographs of polished and etched surfaces of (a) Cr_2AlC; (b) $(Cr_{0.75}V_{0.25})_2AlC$; (c) $(Cr_{0.5}V_{0.5})_2AlC$; (d) $(Cr_{0.25}V_{0.75})_2AlC$; (e) V_2AlC.

https://doi.org/10.1557/jmr.2014.91 Published online by Cambridge University Press

TABLE III. Typical properties of the as-prepared $(Cr_{1-x}V_x)_2AlC$ solid solutions.

Properties	Average grain size (μm)	Aspect ratio	Flexural strength (MPa)	Fracture toughness (MPa $m^{1/2}$)	Hardness (GPa)
Cr_2AlC	17.9 ± 2.1	1.4 ± 0.1	303 ± 5	4.87 ± 0.05	4.14 ± 0.09
$(Cr_{0.75}V_{0.25})_2AlC$	17.6 ± 2.4	1.7 ± 0.1	343 ± 8	5.26 ± 0.09	4.60 ± 0.06
$(Cr_{0.5}V_{0.5})_2AlC$	18.7 ± 1.9	2.1 ± 0.2	402 ± 7	5.91 ± 0.09	5.18 ± 0.07
$(Cr_{0.25}V_{0.75})_2AlC$	18.8 ± 2.3	2.5 ± 0.1	354 ± 10	5.43 ± 0.08	4.64 ± 0.08
V_2AlC	19.5 ± 2.5	3.2 ± 0.3	273 ± 6	4.73 ± 0.07	3.75 ± 0.10

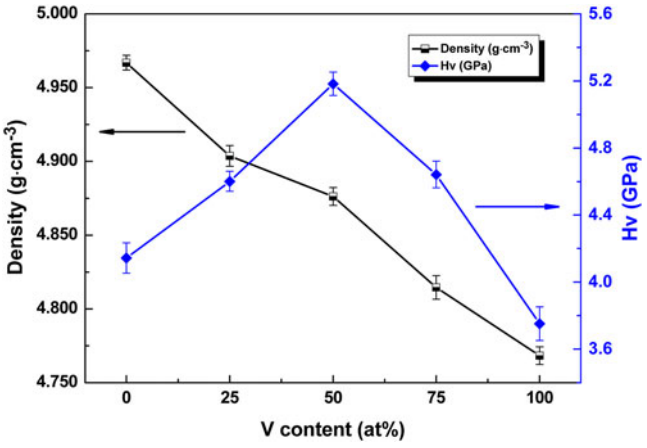


FIG. 7. The density and Vickers hardness of bulk $(Cr_{1-x}V_x)_2AlC$ solid solutions with different V content.

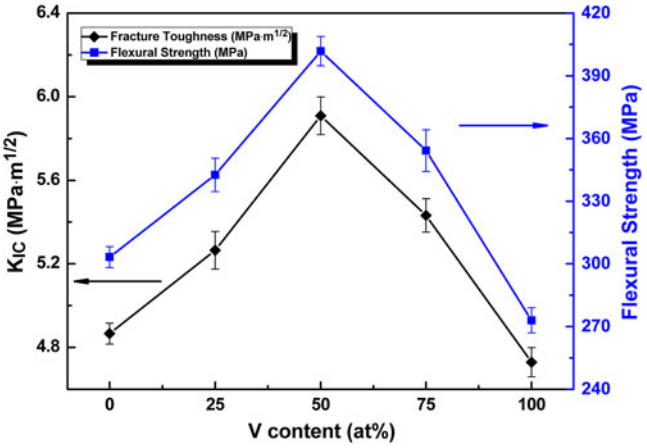


FIG. 8. The flexural strength and fracture toughness of bulk $(Cr_{1-x}V_x)_2AlC$ solid solutions with different V content.

reached a maximum value of 5.18 GPa when the V content was 50 at.%, which was 25.1% and 38.1% higher than that of Cr_2AlC (4.14 GPa) and V_2AlC (3.75 GPa), respectively. These results were partly in accordance with that of Tian's research.[10] But the Vickers hardness of bulk $(Cr_{1-x}V_x)_2AlC$ was larger than the one in their report (4.3 GPa).

The flexural strength and fracture toughness of the $(Cr_{1-x}V_x)_2AlC$ solid solutions with different V content are shown in Fig. 8. Dramatically, the dependence of these two mechanical properties on the V content had a similar tendency with that of the Vickers hardness. The mechanical properties of the $(Cr_{1-x}V_x)_2AlC$ solid solutions are summarized in Table III. Comparing to the pure Cr_2AlC and V_2AlC, the flexural strength of the $(Cr_{0.5}V_{0.5})_2AlC$ solid solution was increased by 32.7% and 47.3%, respectively. Likewise, the value of fracture toughness of the $(Cr_{0.5}V_{0.5})_2AlC$ solid solution was increased by 21.4% and 24.9% when compared with Cr_2AlC and V_2AlC, respectively. Based on the results, $(Cr_{0.5}V_{0.5})_2AlC$ was determined to be a solid solution with the optimal mechanical performance. This phenomenon of strengthening and toughening of was credited to a combined solid solution effect of two factors. On the one hand, the morphology of grains played a major role in modifying the mechanical properties, since there was no distinct difference between the average grain size of $(Cr_{1-x}V_x)_2AlC$ solid solutions. When the V content on the M site was 50%, the aspect ratio of $(Cr_{0.5}V_{0.5})_2AlC$ grains reached about 2.1, a relatively large value. And its grains turned into a transitional shape between the hexagonal and long-columnar morphology. Such a qualitative change presumably had positive influence on improving the mechanical properties. On the other hand, according to the similar theory of alloy solid solutions,[27] it could be concluded that, when the concentrations of Cr and V on the M site simultaneously reached 50 at.% in the $(Cr_{1-x}V_x)_2AlC$ system, the size misfit between Cr and V atoms would cause more lattice distortions and local stress fields. So the dislocation motion was impeded by more interactions between dislocations and local stress fields, which would lead to the maximum solid solution strengthening effect in the $(Cr_{0.5}V_{0.5})_2AlC$ ceramic.

IV. CONCLUSIONS

$(Cr_{1-x}V_x)_2AlC$ ceramics have been successfully synthesized at 1400 °C by in situ hot-pressing method based on the Cr–V–Al–C system. The as-prepared compounds were nearly dense and the average grain size was about 17.9–19.5 μm. The formation process included the production and phase equilibriums of intermetallics, reactions between C and intermetallics, together with the generation of solid solutions. The lattice constants of $(Cr_{1-x}V_x)_2AlC$ increased with the increment of V content. The grains of

https://doi.org/10.1557/jmr.2014.91 Published online by Cambridge University Press

$(Cr_{1-x}V_x)_2AlC$ solid solutions changed from equiaxial to elongated morphology with increasing the V content. The energy-consuming mechanisms in the $(Cr_{1-x}V_x)_2AlC$ solid solutions would contribute to their high toughness and ductility. Moreover, the $(Cr_{0.5}V_{0.5})_2AlC$ solid solution had a combination of high flexural strength of 402 MPa, high fracture toughness of 5.91 MPa $m^{1/2}$, and high Vickers hardness of 5.18 GPa, due to the solid solution effect.

ACKNOWLEDGMENTS

This work was supported by the National Foundation of Natural Science, China (51272145, 51171096), the Shaanxi Provincial Foundation of Natural Science, China (2010JM6014), and the Graduate Innovation Fund of Shaanxi University of Science and Technology.

REFERENCES

1. M.W. Barsoum: The $M_{n+1}AX_n$ phases: A new class of solids; thermodynamically stable nanolaminates. *Prog. Solid State Chem.* **28**, 201 (2000).
2. J.C. Schuster, H. Nowotny, and C. Vaccaro: The ternary systems: Cr-Al-C, V-Al-C, and Ti-Al-C and the behavior of H-Phases (M_2AlC). *J. Solid State Chem.* **32**(2), 213 (1980).
3. C.F. Hu, H.B. Zhang, F.Z. Li, Q. Huang, and Y.W. Bao: New phases' discovery in MAX family. *Int. J. Refract. Met. Hard Mater.* **36**, 300 (2013).
4. W.B. Tian, P.L. Wang, G.J. Zhang, Y.M. Kan, Y.X. Li, and D.S. Yan: Synthesis and thermal and electrical properties of bulk Cr_2AlC. *Scr. Mater.* **54**(5), 841 (2006).
5. G.B. Ying, X.D. He, M.W. Li, W.B. Han, F. He, and S.Y. Du: Synthesis and mechanical properties of high-purity Cr_2AlC ceramic. *Mater. Sci. Eng., A* **528**(6), 2635 (2011).
6. T.T. Ai: High-temperature oxidation behavior of un-dense Ti_3AlC_2 material at 1000 °C in air. *Ceram. Int.* **38**(3), 2537 (2012).
7. Z.J. Lin, M.S. Li, J.Y. Wang, and Y.C. Zhou: High-temperature oxidation and hot corrosion of Cr_2AlC. *Acta Mater.* **55**(18), 6182 (2007).
8. L.O. Xiao, S.B. Li, G.M. Song, and W.G. Sloof: Synthesis and thermal stability of Cr_2AlC. *J. Eur. Ceram. Soc.* **31**(8), 1497 (2011).
9. I.M. Low, W.K. Pang, S.J. Kennedy, and R.I. Smith: High-temperature thermal stability of Ti_2AlN and Ti_4AlN_3: A comparative diffraction study. *J. Eur. Ceram. Soc.* **31**, 159 (2011).
10. W.B. Tian, Z.M. Sun, H. Hashimoto, and Y.L. Du: Synthesis, microstructure and properties of $(Cr_{1-x}V_x)_2AlC$ solid solutions. *J. Alloys Compd.* **484**, 130 (2009).
11. I. Salama, T. El-Raghy, and M.W. Barsoum: Synthesis and mechanical properties of Nb_2AlC and $(Ti,Nb)_2AlC$. *J. Alloys Compd.* **347**, 271 (2002).
12. F.L. Meng, Y.C. Zhou, and J.Y. Wang: Strengthening of Ti_2AlC by substituting Ti with V. *Scr. Mater.* **53**(12), 1369 (2005).
13. M.W. Barsoum, M. Ali, and T. El-Raghy: Processing and characterization of Ti_2AlC, Ti_2AlN and $Ti_2AlC_{0.5}N_{0.5}$. *Metall. Mater. Trans. A* **31**(7), 1857 (2000).
14. S.B. Li, G.P. Bei, C.W. Li, M.X. Ai, H.X. Zhai, and Y. Zhou: Synthesis and deformation microstructure of $Ti_3SiAl_{0.2}C_{1.8}$ solid solution. *Mater. Sci. Eng., A* **441**, 202 (2006).
15. M.X. Ai, H.X. Zhai, Y. Zhou, Z.Y. Tang, Z.Y. Huang, Z.L. Zhang, and S.B. Li: Synthesis of Ti_3AlC_2 powders using Sn as an additive. *J. Am. Ceram. Soc.* **89**(3), 1114 (2006).
16. A. Ganguly, T. Zhen, and M.W. Barsoum: Synthesis and mechanical properties of Ti_3GeC_2 and $Ti_3(Si_xGe_{1-x})C_2$ ($x = 0.5, 0.75$) solid solutions. *J. Alloys Compd.* **376**, 287 (2004).
17. M. Radovic, A. Ganguly, and M.W. Barsoum: Elastic properties and phonon conductivities of $Ti_3Al(C_{0.5},N_{0.5})_2$ and $Ti_2Al(C_{0.5},N_{0.5})$ solid solutions. *J. Mater. Res.* **23**(6), 1517 (2008).
18. J.Y. Wang and Y.C. Zhou: Ab initio elastic stiffness of nanolaminate $(M_xM'_{2-x}AlC)AlC$ (M and M′ = Ti, V, Cr) solid solution. *J. Phys.: Condens. Matter* **16**, 2819 (2004).
19. Z. Sun, R. Ahuja, and J.M. Schneider: Theoretical investigation of the solubility in $(M_xM'_{2-x}AlC)AlC$ (M and M′ = Ti, V, Cr). *Phys. Rev. B* **68**(22), 224112 (2003).
20. C.L. Yeh and W.J. Yang: Formation of MAX solid solutions $(Ti,V)_2AlC$ and $(Cr,V)_2AlC$ with Al_2O_3 addition by SHS involving aluminothermic reduction. *Ceram. Int.* **39**(7), 7537 (2013).
21. W.B. Yu, S.B. Li, and W.G. Sloof: Microstructure and mechanical properties of a $Cr_2Al(Si)C$ solid solution. *Mater. Sci. Eng., A* **527**, 5997 (2010).
22. E. Clementi, D.L. Raimondi, and W.P. Reinhardt: Atomic screening constants from SCF functions. II. Atoms with 37 to 86 electrons. *J. Chem. Phys.* **47**(4), 1300 (1967).
23. M.W. Barsoum, A. Murugaiah, S.R. Kalidindi, T. Zhen, and Y. Gogotsi: Kink bands, nonlinear elasticity and nanoindentations in graphite. *Carbon* **42**, 1435 (2004).
24. A.G. Zhou and M.W. Barsoum: Kinking nonlinear elastic deformation of Ti_3AlC_2, Ti_2AlC, $Ti_3Al(C_{0.5},N_{0.5})_2$ and $Ti_2Al(C_{0.5},N_{0.5})$. *J. Alloys Compd.* **498**(1), 62 (2010).
25. C.F. Hu, F.Z. Li, L.F. He, M.Y. Liu, J. Zhang, J.M. Wang, Y.W. Bao, J.Y. Wang, and Y.C. Zhou: In situ reaction synthesis, electrical and thermal, and mechanical properties of Nb_4AlC_3. *J. Am. Ceram. Soc.* **91**(7), 2258 (2008).
26. C.F. Hu, L.F. He, M.Y. Liu, X.H. Wang, J.Y. Wang, M.S. Li, and Y.W. Bao, and Y.C. Zhou: In situ reaction synthesis and mechanical properties of V_2AlC. *J. Am. Ceram. Soc.* **91**(12), 4029 (2008).
27. Ø. Ryen, B. Holmedal, O. Nijs, E. Nes, E. Sjölander, and H.E. Ekström: Strengthening mechanisms in solid solution aluminum alloys. *Metall. Mater. Trans. A* **37**(6), 1999 (2006).

https://doi.org/10.1557/jmr.2014.91 Published online by Cambridge University Press